Journal of Applied Mechanics and Technical Physics, Vol. 38, No. 6, 1997

AN EXPERIMENTAL AND NUMERICAL STUDY OF ACOUSTIC FLOWS NEAR CAVITY RESONATORS

A. A. Aganin,[1] V. B. Kuznetsov,[1]
E. V. Martynov,[2] and E. T. Smirnova[1]

UDC 534.2:532

When a cavity resonator (acoustic resonator, Helmholtz resonator) is excited, acoustic flow (acoustic streaming and acoustical wind) occurs [1–5]. The papers devoted to this phenomenon are few in number [6–9]. At the same time, acoustic flow has some useful practical applications. In particular, in discontinuous-flow chambers, it can be used to produce gas flows, which ensure mixing of the media or increase the heat exchange of structural members inside the chambers without introduction of additional masses of gases, mixers, etc. into the working space [6], and to decrease the body drag in flow [8]. The acoustic flow phenomenon is used to develop a new class of electropneumatic converters [10, 11] that are distinguished by the absence of members working with friction.

The present paper reports the results of an experimental and numerical study of acoustic flow near excited cavity resonators having small dimensions (volume < 1 cm^3) and a short length of the channel orifice ($\delta < 0.1$ mm). We study cylindrical resonators with a diameter of the cylinder of 15 to 50 mm and a diameter of the channel of 1.2 to 5 mm. The excitation is harmonic. The source of excitation functions as the walls of the resonator. The goal of the study is to determine the dependence of the acoustic-flow characteristics on the excitation parameters and geometry of the resonators, to analyze a numerical model of the excitation of acoustic flow as applied to the type of resonators studied, and to determine the region of application of this model. Considerable attention was given to the determination and analysis of the resonance regime in which both the acoustic-flow velocity (the velocity of the mean flow along the symmetry axis) in the outer region of the resonator and the amplitude of velocity fluctuations in the orifice reach maximum values. In the experiments, the occurrence of resonance was judged by the signal of a hot-wire anemometer, and, in the calculations, by the amplitude of gas-velocity fluctuations at the center of the orifice.

1. Experimental Studies. *Description of the Experimental Setup.* In the present work, the experimental data were obtained by means of the resonator model shown schematically in Fig. 1. The model includes a body 1, a piezoceramic converter 2, the resonator cavity 3, and a replaceable plate 4 with an orifice 5.

The setup incorporated a TPS-3 (T7-M) high-frequency hot-wire anemometer for measuring the instantaneous value of the gas-flow velocity. The constant component of the velocity (or the velocity averaged over the period of oscillations of the piston, called "average" below) is measured by a low-frequency hot-wire anemometer, developed and produced at the Research Laboratory "Measuring Converters" of the Tupolev Kazan' State Technical University. During the experiments, signals from the hot-wire anemometers were measured by an F30 (F386) digital voltmeter with an accuracy class of 0.2.

The sensitive element of high-frequency hot-wire anemometers, intended for the measurement of the variable velocity components, is a tungsten microwire 2 μm in diameter and 500 μm long. The bandwidth of hot-wire anemometers with such a sensitive element reaches 1500 Hz at a 100% degree of flow modulation and zero constant velocity. A microwire of the required thickness was obtained by the electrochemical polishing technology. The sensitive element of the low-frequency hot-wire anemometer is a CT1-18 semiconducting temperature-sensitive resistor with a 0.2-mm-diameter working part.

[1]Institute of Mechanics and Engineering, Kazan' Scientific Center, Kazan' 420111. [2]Tupolev Kazan' State Technical University, Kazan' 420111. Translated from Prikladnaya Mekhanika i Tekhnicheskaya Fizika, Vol. 38, No. 6, pp. 61–71, November–December, 1997. Original article submitted April 22, 1996.

 0021-8944/97/3806-0868 $18.00

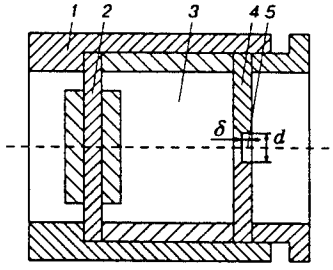

Fig. 1

The sensitive elements of the hot-wire anemometer are displaced, by means of micrometric screws with an accuracy of 0.01 mm, in three mutually perpendicular directions in the flow relative to the tested model.

The velocity head was measured by MMI-240 inclined-tube alcohol manometers and electron absolute-pressure gauges of the DDG type. The miniature Pitot head used had an inlet port of 0.2 mm diameter and a working part of diameter 0.5 mm. Sinusoidal voltage from a G3-56/1 audio-signal generator was delivered to the piezoceramic converter of the model.

Before each cycle of measurements, we calibrated the sensitive elements of the hot-wire anemometers. Calibration at velocities lower than 10 m/sec was performed on a rotary calibration setup. Calibration at velocities higher that 10 m/sec was performed using a special selector of the reference flow. The blower of the selector produces air flow through a profiled nozzle. The calibrated sensitive element and the miniature Pitot head connected to the manometers were placed in the laminar core of the nozzle exit flow. The reference velocity was calculated from the readings of the manometers. The volume amplitude of oscillations of the piezoceramic converter is determined by recalculation of the results from measurements of the oscillation amplitude at several points on the surface of the electroacoustic radiator along the diameter of the radiator. The measurements were performed by an optical method using a cathetometer.

Experimental Results. Below we give the results that correspond to the excitation of the resonator at the natural frequency Ω, which is determined from the relation

$$\Omega = c_0\sqrt{\frac{S}{\delta+\delta^*}\left(\frac{1}{V}+\frac{1}{V_{\text{out}}}\right)}$$

if we set $V_{\text{out}} \to \infty$. Here c_0 is the sound velocity in the unperturbed gas, S is the surface area of the orifice, δ is the channel length, δ^* is the end correction (for the resonator geometry considered, we can assume that $\delta^* = 0.85d$), V is the volume of the resonator cavity, and V_{out} is the volume of the outer cavity with which the resonator is connected through the orifice. This relation for Ω can be obtained if we consider a resonant system with concentrated parameters, assuming that the mass is concentrated in the orifice, and the elasticity is concentrated in cavities. For the resonator geometry, $\delta^* = 0.85d$. This value is obtained in accordance with [12] and is confirmed experimentally.

Our studies show that the acoustic flow in the vicinity of small-size resonators with a small length of the channel orifice is of the form of a vortex flow with a pulsating jet directed along the symmetry axis from the resonator to the outer region. Laminar, transition, or turbulent regimes are observed, depending on the excitation parameters and the resonator geometry.

For sufficiently large diameters ($>10d$) and lengths of the resonator cavity ($>2d$) compared with the diameter of the orifice and for small excitation amplitudes, the laminar regime is established. In the laminar regime, high-frequency random pulsations are absent over the entire flow regions and the jet velocity is small. With increase in the excitation amplitude, the jet velocity increases. Then, transition to another regime occurs: for $\delta/d < 0.02$, to the turbulent regime, and for $\delta/d > 0.02$, to the transition regime. In the first case, the transition proceeds at Reynolds numbers $\text{Re} \approx 600$–800 ($\text{Re} = \langle v\rangle_{\max} d/\nu$, where $\langle v\rangle_{\max}$ is the highest average velocity on the jet axis and ν is the kinematic viscosity coefficient). In the second case, the transition regime occurs earlier. The particular value of Re depends on the ratio δ/d.

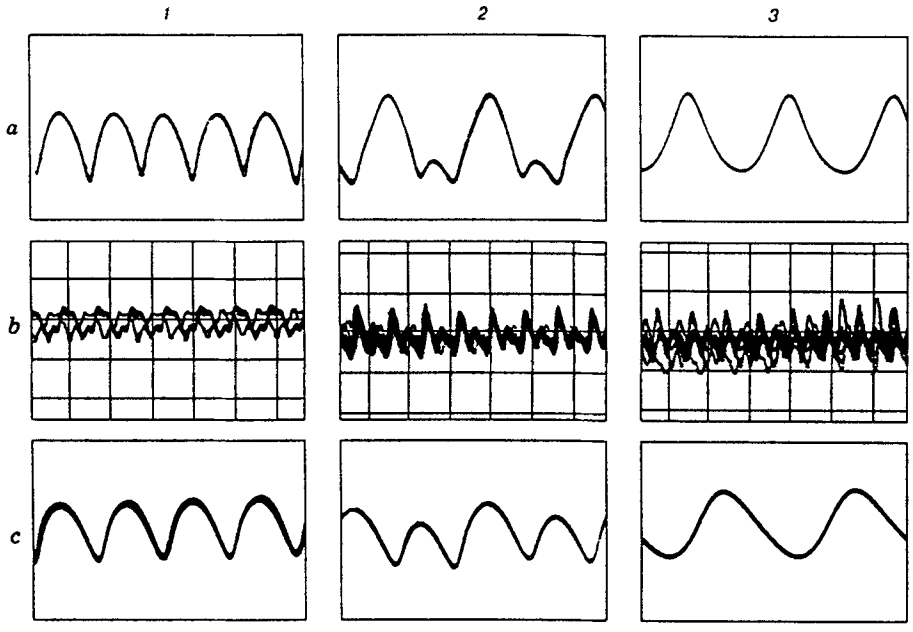

Fig. 2

The transition regime is characterized by the presence of high-frequency chaotic pulsations over the entire flow region. With transformation from the laminar to the transition regime, the jet width considerably increases, and the constant velocity component along the symmetry axis abruptly decreases. With increase in the excitation amplitude in the transition regime, the jet velocity increases. At Re $\approx$ 600–800, transition to the turbulent regime occurs.

The turbulent regime is characterized by the presence of a laminar core with length to $5d$ along the symmetry axis. Around the core there is a plume with random high-frequency pulsations, typical of turbulent flows. At Re $\approx$ 600–800, the profile of the constant velocity component of the laminar core is close to a parabolic profile.

With further increase in the excitation amplitude, the jet velocity increases, and its profile in the laminar core further levels off. At Re $\approx$ 1800–2000, the velocity becomes constant over the entire laminar core of the jet. An even larger increase in the excitation amplitude only leads to an increase in the jet velocity. The flow structure remains unchanged.

Figure 2 shows typical oscillograms of velocity fluctuations on the symmetry axis for the laminar (a), transition (b), and turbulent (c) regimes [at the center of the orifice (1), between the orifice and the maximum of the average velocity (2), and with a distance $5d$ (3)]. Figure 2 illustrates the significant difference of the transition gas-flow regime near the orifice at the symmetry axis from the other regimes. The fundamental harmonics here is superimposed by a complex spectrum of perturbations. Figure 2a shows that, with distance from the orifice, the gas flow becomes more and more unidirectional (the signal is detected in the oscillograms). At the center of the orifice the gas moves, over half the oscillation period, into the resonator and then, over half the period, it moves outward at the same velocity, whereas between the orifice and the maximum of the average velocity the amplitude of the gas velocity toward the resonator is two times lower than the gas velocity outward of the resonator. The oscillations at a distance $5d$ show that the motion of the gas here is completely unidirectional.

Dependence of Acoustic Flow on the Excitation Parameters and Geometric Characteristics of the Resonator. The above results were obtained for the excitation at the natural frequency Ω and with sufficiently large dimensions of the resonator cavity compared with the orifice diameter. With deviations of the excitation frequency ω from Ω over the entire frequency range studied (300–5000) Hz, there are no changes in the Reynolds numbers at which, in the turbulent regime, the profile of the constant-velocity component of the

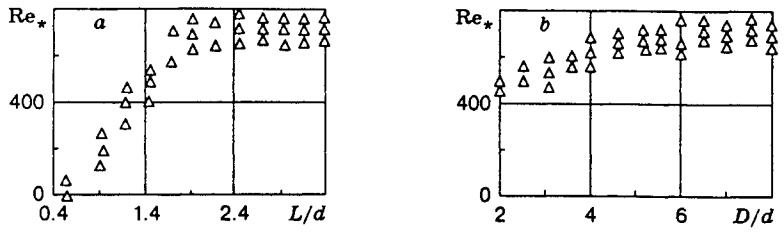

Fig. 3

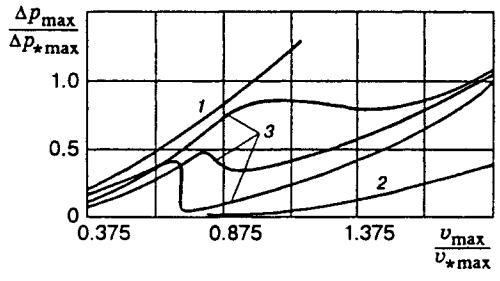

Fig. 4

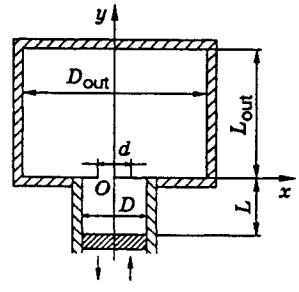

Fig. 5

laminar core of the jet becomes constant. The occurrence of the transition regime depends on the excitation frequency. At $\omega < 0.8\Omega$, the transition regime can be absent, i.e., with increase in the excitation amplitude, the laminar regime immediately becomes turbulent. At $\omega > 1.5\Omega$, the reverse situation is possible. Even at small excitation amplitudes, the transition regime can immediately occur in this case.

It is established that, with increase in the dimensions of the working cavity, the transition Reynolds numbers Re_* that correspond to the transition of the laminar to the transition regime change. Figure 3 gives the generalized dependence of Re_* on the relative length L/d (Fig. 3a) and diameter D/d (Fig. 3.b) of the working cavity. As can be seen, for $L/d > 1.6$ and $D/d > 5$, the value of Re_* remains constant, and with decrease in this parameters, it decreases.

For a fixed geometry of the resonator within the framework of a definite regime of acoustic flow, an increase in the excitation amplitude leads to an increase in the oscillation orifice velocity and the average jet velocity. At the same time, the average jet velocity can change suddenly with transition of one regime to another.

Figure 4 gives the dependence of the dimensionless velocity head $\Delta p_{\max}/\Delta p_{*\max}$ at the maximum of the average jet velocity on the dimensionless amplitude of velocity fluctuations $v_{\max}/v_{*\max}$ at the center of the orifice. Curve 1 corresponds to the case where flow begins in the laminar regime, and, without transforming to the transition regime, becomes turbulent (in this case, the dimensions of the sensitive element were such that it did not react to the perturbed flow beyond the boundaries of the laminar core). Curve 2 corresponds to the flow that begins in the transition regime and then becomes turbulent, and curve 3 shows the case where flow begins in the laminar regime which becomes the transition regime and then the turbulent regime. The parameters $\Delta p_{\max}$ and $v_{\max}$ were made dimensionless with respect to their values $\Delta p_{*\max}$ and $v_{*\max}$ that correspond to the laminar–turbulent transition in curve 1. As can be seen, the occurrence of the transition regime between the laminar and the turbulent regimes leads to the non-single-valued dependence of $\Delta p_{\max}/\Delta p_{*\max}$ on $v_{\max}/v_{*\max}$ (curves 3). It is also interesting to note that curve 1 corresponds to the minimum expenditure of the resonator excitation energy required for the attainment of the given velocity of acoustic flow.

2. Numerical Simulation. *Formulation of the Problem.* Numerical simulation was performed by integration of two-dimensional equations of an inviscid non-heat-conducting gas in mixed Eulerian–Lagrangian variables [13]. The finite-difference method belongs to the class of high-resolution TVD schemes of second-order accuracy with respect to time and space [14]. In the calculations, the cavity resonator is a cylindrical

cavity. On one end of the cavity there is a circular plate with an orifice at the center, and, at the other end there is a flat piston vibrating in the axial direction. The plate and the piston are orthogonal to the symmetry axis. The outer region is bounded by immovable walls, which, together with the surface of the resonator, form an outer cylindrical cavity located uniaxially with the resonator cavity.

The diametral sections of the cavity resonator and the outer cavity are shown in Fig. 5 ($L_{\text{out}}/L = 3$, $D/d = 10$, $D_{\text{out}}/D = 2.5$, and $D/L = 3.75$). The walls and the plate are considered absolutely rigid. The plate is considered infinitely thin. Before the initial time, the gas medium inside the resonator is in a state of rest. At the initial moment, the piston begins to move, exciting the resonator. During some time, transition processes proceed inside the resonator and in the outer cavity. Then, these processes enter a periodically recurring regime.

The law of motion of the piston is given in the form

$$y_p = y_0 + l\sin\omega t, \tag{2.1}$$

where l and ω are the amplitude and angular frequency of oscillations, y_p is the location of the piston at time t, and y_0 is the axial coordinate of the piston for $t = 0$, which corresponds to its middle position ($y_0 = -L$).

Numerical simulation is performed by integrating the two-dimensional equations of an inviscid non-heat-conducting gas, which in Cartesian coordinates can be written in the form of conservation laws as follows:

$$\begin{gathered}\mathbf{u}_t + \mathbf{f}_x + \mathbf{g}_y = \mathbf{s}, \quad \mathbf{u} = (\rho x, \rho x u, \rho x v, xE)^{\mathrm{t}}, \quad \mathbf{f} = (\rho x u, x(p+\rho u^2), \rho x u v, x(p+E)u)^{\mathrm{t}}, \\ \mathbf{g} = (\rho x v, \rho x u v, x(p+\rho v^2), x(p+E)v)^{\mathrm{t}}, \quad \mathbf{s} = (0, p, 0, 0)^{\mathrm{t}}.\end{gathered} \tag{2.2}$$

Here p is the pressure, E is the specific total energy per unit volume, u and v are the components of the gas-particle velocity in the radial Ox and axial Oy directions, α_z is the partial derivative $\partial\alpha/\partial z$, and the superscript t denotes transposition.

System (2.2) is closed by the equation of state

$$p = (\gamma - 1)(E - \rho(u^2 + v^2)/2), \tag{2.3}$$

where γ is the adiabatic exponent ($\gamma = 1.4$).

In problems with moving boundaries, it is more convenient to use equations in mixed Eulerian–Lagrangian variables instead of Eqs. (2.2). In the present work, they are used in the form

$$\begin{gathered}\mathbf{U}_\tau + \mathbf{F}_\xi + \mathbf{G}_\eta = \mathbf{S}, \qquad \mathbf{U} = \frac{\mathbf{u}}{\Delta}, \qquad \mathbf{F} = \frac{\xi_t}{\Delta}\mathbf{u} + \frac{\psi_x}{\Delta}\mathbf{f} + \frac{\xi_y}{\Delta}\mathbf{g}, \\ \mathbf{G} = \frac{\eta_t}{\Delta}\mathbf{u} + \frac{\eta_x}{\Delta}\mathbf{f} + \frac{\eta_y}{\Delta}\mathbf{g}, \qquad \mathbf{S} = \frac{\mathbf{s}}{\Delta},\end{gathered} \tag{2.4}$$

where $\Delta = \partial(\xi,\eta)/\partial(x,y)$, and τ, ξ, and η are mixed Eulerian–Lagrangian variables. The main concepts of the difference scheme used to solve system (2.2)–(2.4) are given in [13].

The boundary conditions on the surface of contact of the gas with the cavity walls and with the movable piston are the nonpenetration conditions. At $t \leqslant 0$, the gas has unperturbed values of density ρ_0, pressure p_0, sound velocity c_0, radial $u_0 = 0$, and axial $v_0 = 0$ components of the velocity vector, etc. At $t = 0$, the piston begins to move into the resonator cavity with a maximum velocity according to the law (2.1).

It is not hard to see that the calculation scheme (Fig. 5) has a number of differences from the model used in the experiments (see Fig. 1).

First, the source of excitation of oscillations in the calculated resonator is a flat piston and not a membrane as in the experiments. Therefore, in comparisons, the membrane is regarded as an "effective" flat piston whose amplitude of displacements is determined from the equality of the displaced volumes.

Second, instead of the plate of finite thickness used in the experiments, the calculations use an infinitely thin, absolutely rigid membrane with an orifice at the center. For comparatively small thicknesses of the plate and a small length of the orifice channel, this replacement seems quite admissible, although the configuration of the plate used in the experiments is only an approximation of the idealization represented by the calculation

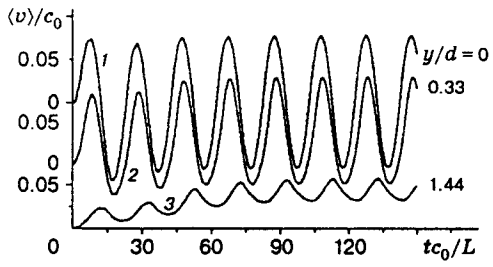

Fig. 6

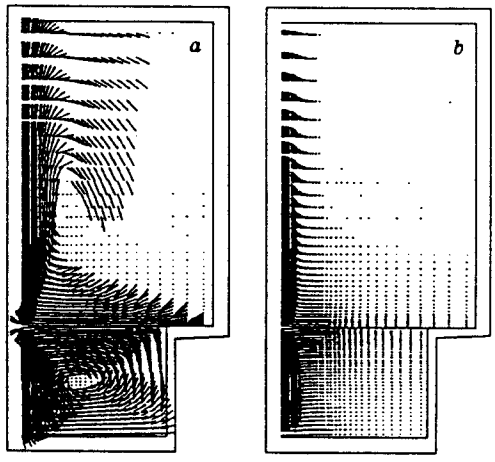

Fig. 7

scheme. In the experiments, the use of a thin plate gave rise to bending oscillations, which introduced uncontrollable deviations into the experimental results. On the other hand, the use of a thick plate increased the length of the orifice channel, leading to large frictional losses of energy.

Third, the outer region in the calculation scheme is bounded, and there are no restrictions in the experiments. However, experiments showed that, as the dimensions of the outer cavity of the resonator increase (with respect to the dimensions of the orifice), the effect of this cavity on the processes near the orifice can be ignored.

Thus, it appears that, despite the indicated differences, a qualitative comparison of gas-dynamic processes in the calculations and experiments is possible.

Calculation Results. The calculation region is divided into four zones by the straight lines $y = 0$ and $x = r = d/2$ with the number of cells I_k along the radial direction and the number of cells J_k along the axial direction, where $k = \overline{1,4}$ is the zone number. It is assumed that zones 1–4 are in the regions $\{x \leqslant r, y \leqslant 0\}$, $\{x \geqslant r, y \leqslant 0\}$, $\{x \leqslant r, y \geqslant 0\}$, and $\{x \geqslant r, y \geqslant 0\}$, respectively. In addition, $I_1 = I_3$, $J_1 = J_2$, and $J_3 = J_4$. The finite-difference grid consists of rectangular cells. Along the radius in zones 1 and 3, the grid is uniform with a step r/I_1, and, in zones 2 and 4, it is expanded from the orifice in geometric progression with the first element equal to r/I_1. Along the axial direction in all zones, the grid is expanded from $y = 0$ in the geometric progression with the first element equal to r/I_1. In zones 1 and 2, where the grid is movable because of displacements of the piston, the grid is rearranged so that the denominator of the progression remains unchanged.

We examine the case $l/L = 0.01$ and $\omega L/(2\pi c_0) = 0.05$. Numerical convergence was estimated using the following grids: $I_1 = 10/13/16/20/25/31$, $I_2 = 35/40/44/48/52/56$, $I_4 = 40/45/49/54/58/62$, $J_1 = 27/31/34/38/42/46$, and $J_3 = 45/50/54/59/63/67$. The number of cells in the orifice of each next finer grid $I_1 = I_3$ was assumed to be $\approx$1.25 times larger than in the previous grid. Moreover, all the expansion coefficients used were considered equal to $\approx$1.05.

Time dependences of the instantaneous velocity at the center of the orifice and distributions of the axial component of the average velocity vector along the symmetry axis were obtained on different grids and analyzed. Analysis shows that the curves of the average velocity differ more widely. This indicates the important role of the cell size for the qualitative description of the transition of the gas oscillations in the orifice to unidirectional motion (jet) near the orifice. At the same time, comparison of the flow structure on different grids shows that the qualitative features (which are considered below) of the numerical solution on the finest grid also takes place on coarser grids.

The formation of jet flow in time is illustrated in Fig. 6, which shows the time dependences of the instantaneous velocity at individual points of the symmetry axis. The figure also shows the following

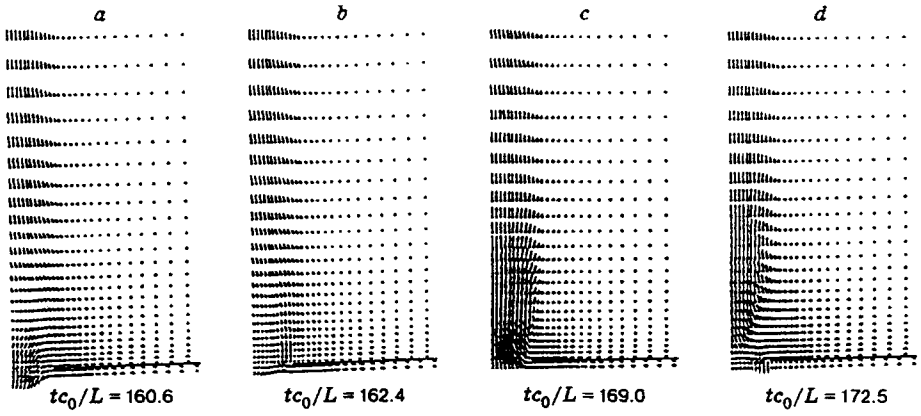

Fig. 8

characteristic feature of the experimental results (see Fig. 2): over half the period, the gas flows through the orifice into the resonator, and, over half the period, it flows outward of the resonator (curve 1); with displacement of the wall toward the outer region, the motion toward the resonator decreases (curve 2), and, beginning with a certain distance, the flow becomes completely unidirectional (curve 3).

As can be seen from Fig. 6, within the framework of the adopted formulation of the problem, the transition processes near the orifice terminates after 3 or 4 oscillations. The periodic regime near the far (from the orifice) wall of the outer cavity is attained over a larger period of time (about 10 oscillations).

The structure of the mean flow, which is established in the calculations after the completion of transition processes in the resonator and in the outer cavity, completely agrees with the experimental data. The vectors of equal length in Fig. 7a show streamlines of the mean flow. The direction of these vectors is governed by the fact that, in the resonator (in the outer cavity), the gas rotates counterclockwise (clockwise), and the point instead of the vector means that the absolute value of the velocity here is small. Figure 7b shows the field of the average-velocity vectors. It can be seen from Fig. 7 that in both cavities the gas performs vortex motion with the velocity directed toward the orifice near the plate. The flow near the symmetry axis is of a jet character. Inside the resonator, the jet is directed toward the piston, and, outside, it is oppositely directed.

Comparison of the calculated distribution of the axial component of the jet average velocity in various sections with distance from the orifice and the experimental data shows that the calculated curves agree with the case of the laminar regime (with distance from the orifice, the jet is expanded) and do no reflect the flow features associated with changes of the flow regime. The calculation model does not incorporate any mechanisms that take into account turbulence.

The gas-dynamic processes that occur in the outer cavity near the orifice during one period of piston oscillations are illustrated in Fig. 8, which shows the velocity-vector fields at some characteristic times in a fragment of the calculation region, bounded from the left by the symmetry axis. The fragment covers part of the wall (the solid horizontal straight line) and two layers of cells adjacent to the wall from the inner side of the resonator. The points show the vector origins.

The flow through the orifice of the cavity resonator can be divided into two phases: suction of the gas in the resonator and ejection into the outer cavity. The first phase corresponds to the half-period in which the orifice velocity is negative, and the second corresponds to the half-period with the velocity directed from the resonator cavity to the outer cavity.

Figure 8a shows the time that corresponds to the developed phase of suction. The gas flows in the resonator from both the region above the orifice and from the zone adjacent to the plate edge. In the remaining portion of the outer cavity, the velocity is small everywhere, except for the zone near the symmetry axis, where the gas moves upward.

With time, the suction phase becomes weaker, and transition to the ejection phase occurs (Fig. 8b). A characteristic feature of this transition is that, at various places of the orifice, the gas moves in different

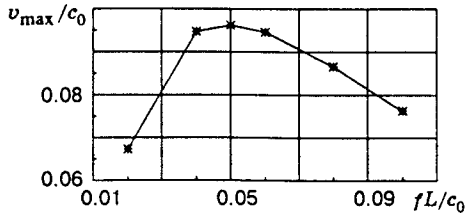

Fig. 9

directions. Near the axis, the gas particles continue to move to the resonator cavity, whereas near the orifice edge the gas begins to flow outward to the outer cavity. The main changes have occurred in the zone near the orifice at a distance $<1d$. The values and distributions of the jet velocity vectors at a large distance from the orifice have changed only slightly.

After a short time, the transition to the ejection phase ends. The developed state of this phase is shown in Fig. 8c. Comparison with Fig. 8b shows that the main changes again occurred in the zone near the orifice. The velocities here have increased considerably and are the highest for the entire flow region shown in the figure. At the same time, the upper part of the fragment "reacts" weakly to the processes near the orifice. The value and distribution of the velocity vectors do not change markedly here.

In what follows, the ejection attenuates. Transition of ejection to suction occurs (Fig. 8d). And again the flow (now to the resonator cavity) begins near the edge of the orifice. The highest velocities are located on the symmetry axis at $\approx 1.5d$ from the orifice, and this is a consequence of the ejection.

After a time, a pattern similar to that shown in Fig. 8a is established, and, in what follows, the process recurs.

Effect of the Geometric Characteristics and Excitation Parameters. The calculations show that small deviations of the geometrical dimensions of the resonator and the outer cavity (with respect to the orifice diameter) and the frequencies and amplitudes from those numerical values for which the above results are obtained do not lead to qualitative changes in the acoustic flow characteristics.

A calculation for $L_{out}/L = 2$ was performed to estimate the effect of the dimensions of the outer cavity. Comparison of the distribution of the axial component of the average velocity vector along the symmetry axis for $L_{out}/L = 2$ and $L_{out}/L = 3$ shows that, inside the resonator and in the outer cavity up to $y/L = 1.0$, the curves diverge insignificantly. It is, therefore, concluded that the results reported for the near region near the orifice are valid for $L_{out}/L \geqslant 3$.

The effect of the excitation amplitude on the average-velocity distribution along the symmetry axis was estimated from the calculation results for $l/L = 0.005$ and 0.01. It is established that, with decrease in the excitation amplitude, the maximum of the velocity becomes more pronounced and is shifted toward the orifice, and this agrees with the experimental results.

Analysis of the experimental measurements shows that, with variation in the excitation frequency at a constant amplitude, the oscillation velocity in the orifice has a pronounced maximum in the frequency region Ω. Figure 9 shows a similar dependence obtained by calculations. A maximum is observed at the frequency $\omega L/(2\pi c_0) = 0.05$. Calculations using the relation for Ω gives a resonance frequency $\omega L/(2\pi c_0) = 0.061$. Thus, the difference does not exceed 19%.

In summary, we draw the following conclusions. The experimental and numerical studies show that the acoustic flow near the orifice of the cavity resonator is the vortex motion of the gas with the formation of two pulsating buoyant jets along the symmetry axis. Inside the resonator, the jet is directed toward the piston, and, in the outer cavity, it is directed from the orifice to its far wall.

It is established experimentally that, depending on the excitation parameters and the resonator geometry, three possible flow regimes are possible: laminar, transition, and turbulent. Features of these flow regimes are established. Boundaries of transitions from one regime to another and their dependences on the geometrical characteristics of the resonator and excitation parameters are established.

Comparison between the calculation and experimental results shows that the numerical model based on integration of the equations of an inviscid non-heat-conducting gas describes qualitatively well the acoustic-flow structure in the laminar flow regions. In particular, qualitative comparison of the calculation and experimental data pertaining to the laminar regime shows satisfactory agreement between the distribution features: the constant component (averaged over the period) of the velocity along the symmetry axis and radius of the cavity, the time dependences of fluctuations of the instantaneous velocity along the symmetry axis, and the amplitude of the velocity fluctuations in the orifice at the resonance frequency Ω.

The variation in the flow structure near the resonator orifice over one period of oscillations in the steady regime is shown numerically. It is established that the transition of the gas suction in the resonator cavity to the gas ejection to the outer region (and vice versa) begins near the orifice edge. Then, the direction of the gas flow is also reversed in the zone adjacent to the symmetry axis.

This work was supported by the Russian Foundation for Fundamental Research (Grant No. 96-01-00484).

REFERENCES

1. W. L. Nyborg, "Acoustical streaming," in: B. Mason (ed.), *Physical Acoustics*, Vol. 2, Part B, New York (1965).
2. L. K. Zarembo and V. A. Krasil'nikov, *Introduction to Nonlinear Acoustics* [in Russian], Nauka, Moscow (1966).
3. U. Ingard and H. Ising, "Acoustic nonlinearity of an orifice," *J. Acoust. Soc. Am.*, **42**, No. 1, 6–17 (1967).
4. L. K. Zarembo, "Acoustical flows," in: *Strong Ultrasonic Fields. Ser. Physics and Technology of Ultrasound* [in Russian], Nauka, Moscow (1968), pp. 87–128.
5. Z. A. Gol'dberg, "Acoustic wind," in: *Physical Encyclopedic Dictionary* [in Russian], Vol. 1, Sov. Encycl., Moscow (1960), p. 38.
6. E. P. Mednikov and B. G. Novitskii, "An experimental study of a powerful acoustic wind," *Akust. Zh.*, **21**, No. 2, 245–249 (1975).
7. I. V. Lebedeva, "Experimental studies of acoustic flow in the vicinity of an orifice," *Akust. Zh.*, **21**, No. 2, 245–249 (1975).
8. X. Ming and C. H. Dai, "A new phenomenon of acoustic streaming," in: *Proc. Int. Conf. on Dynamic Measurement and Its Applications*, Beijing (1989), pp. 469–476.
9. S. P. Dragan and I. V. Lebedeva, "Analysis of the field structure near the orifice with passage of an intense acoustic wave," in: *Proc. 10th Anniversary Scientific-Research Conference on Aeroacoustics* (Suzdal', September 1992) [in Russian], Part 1, Moscow (1992), p. 136–139.
10. E. V. Martynov, "Characteristics of an electropneumatic measuring converter based on the acoustic streaming phenomenon," in: *Dynamic Measurements, Abstracts 5th All-Union Symp.* [in Russian], VNIIM, Leningrad (1988), p. 52–55.
11. E. V. Martynov and Yu. N. Krasnov, "Piezoelectric electropneumatic converter based on acoustic streaming," in: *New Electron Devices and Facilities, Proc. Conf.* [in Russian], MDNTP, Moscow (1988).
12. U. Ingard, "On the theory and design of acoustic resonators," *J. Acoust. Soc. Am.*, **25**, No 6, 1037–1061 (1953).
13. A. A. Aganin and M. A. Ilgamov, "Numerical simulation of gas oscillations and flows generated by wave resonators," in: *Proc. Int. Conf. on the Methods of Aerophys. Research*, Part 1, Novosibirsk (1994), pp. 3–8.
14. A. Harten, B. Engquist, S. Osher, and S. Chakravathy, "Uniformly high order accurate essentially nonoscillatory schemes. III," *J. Comp. Phys.*, **71**, 231–303 (1987).